UNSYS digital

J Unmanned Sys Tech, 2014, Vol. 2

Design and Development of Fixed-Wing Nano Air Vehicle

Jinraj V Pushpangathan, Karthik S, and M Seetharama Bhat

Indian Institute of Science, Bangalore, India

***Abstract*—**Flight dynamics modeling and analysis of a fixed-wing nano air vehicle (NAV) is studied. In the process of developing a NAV, this paper explains longitudinal and lateral dynamics and performance analysis of 75 mm wing span NAV. The performance and trim analysis are carried out with aerodynamic data found by simulating a typical nano air vehicle geometric configuration in XFLR5 and integrating this data with Matlab. Longitudinal and lateral dynamics are analyzed both for coupled and uncoupled model, and the difference is projected by considering only aerodynamic coupling.

***Keywords*—**Nano air vehicle, phugoid mode, spiral mode, lateral-longitudinal coupling.

I. Introduction

DESIGN and development of very small aircraft for the special missions began seriously in 1996 [1]. This type of small aircraft will carry a variety of payloads such as visual, nuclear, biological, chemical and acoustic sensors. Such vehicles are called micro air vehicles (MAVs). As technology and time progress, the MAV gets reduced to a very small size. Therefore, the design and development of a new class of very small micro air vehicles called nano air vehicle (NAV) has become an interesting subject in future technology. NAV is defined by its dimension by having length, breadth or height less than or equal to 75 mm, and is required to be able to perform various civil-military missions at an affordable cost with gross take-off weight between 10 to15 grams. In general, NAVs serve as innovative technology drivers for realizing increasingly miniature subsystems, which together are capable of achieving complex tasks similar to MAV. The predominant missions of NAVs are primarily the Intelligence, Surveillance and Reconnaissance. The diminutive size and weight of the NAV require advancements in aerodynamic design for low Reynolds number airfoils, lightweight, and efficient propulsion and energy storage systems, autonomous guidance, control, navigation, sensors, and communication subsystems. Simultaneously, advanced manufacturing techniques are also required to achieve the high level of system integration. Major challenges in modeling and analysis of NAVs include low Reynolds number high angle-of-attack flight regimes and vehicle's sensitivity to atmospheric turbulence [1]. Other important technological challenges for developing navigation, guidance and control for NAV are to develop algorithms and techniques that cope with various uncertainties associated with the vehicle's model. Other technical challenges related to hardware is to integrate navigation, guidance and control functions onto a single chip to meet the restrictive size, weight, and power requirements driven by the NAV's mission.

Corresponding author: J. V. Pushpangathan (e-mail: jinrajaero@gmail.com).
This paper was submitted on November 29, 2013; revised on February 4, 2014; and accepted on May 11, 2014.

In the process of developing a fixed-wing NAV which can fit inside a cube of dimension 75 mm, this paper presents longitudinal and lateral dynamics and performance analysis of a 75 mm NAV. The velocity range of NAV is between 7 $m \cdot s^{-1}$ and 12 $m \cdot s^{-1}$. The nano air vehicle is designed using custom-designed airfoil that is optimized for good aerodynamic performance. This paper mainly deals with analysis of coupled and decoupled lateral and longitudinal equations of motion. Six degrees of freedom of rigid-body equations of motion linearized using small disturbance theory are used for flight mechanics analysis [2]-[4]. Lateral and longitudinal equations of motion are decoupled from each other by excluding all cross-coupling terms from linearized six degrees of freedom rigid-body equations of motion. Inertial, gyroscopic, and aerodynamic effects can produce coupling between lateral and longitudinal equations of motion, even under a small disturbance condition. Inertial coupling occurs if the aircraft has an asymmetric mass distribution about X-Z, X-Y, and Y-Z plane. The gyroscopic coupling occurs as a result of any net angular momentum associated with rotors that spin relative to the body-fixed coordinate system. Aerodynamic coupling is indicated by some of the aerodynamics derivatives such as $C_{l,\alpha}$, $C_{L,\beta}$, $C_{n,\alpha}$, $C_{m,\beta}$, etc., being non-zero. Here, $C_{l,\alpha}$ symbolizes rolling moment coefficient derivative with respect to angle-of-attack (rad^{-1}), $C_{L,\beta}$ denotes the lift coefficient derivative with respect to side-slip angle (rad^{-1}), $C_{n,\alpha}$ is the yawing moment coefficient derivative with respect to angle-of-attack (rad^{-1}), and $C_{m,\beta}$ denotes pitching moment coefficient derivative with respect to side-slip angle (rad^{-1}) [5]. The importance of lateral and longitudinal coupling for nano flight is investigated in this paper by considering inertial and aerodynamic coupling while excluding the effect of the propeller on them.

This paper is arranged as follows: section II presents design of NAVs. Nonlinear equations of motion are explained in section 0. Section IV describes linear equations of motion. Simulation results and discussion are carried out in section V.

II. Design Of Nano Air Vehicle

Diagram of the 75 mm NAV drawn using Solidwork software is shown in **Figure 1**. SolidWorks software is used to find inertia parameters of the vehicle. NAV has X-Z plane of symmetry which means that the left side of the NAV is a mirror image of the right side about X-Z plane. This brings J_{xy} and J_{yz} to zero values. The J_{xz} is not necessarily zero because the NAV

is not symmetrical from top to bottom about the X-Y plane and not symmetrical from front to rear about the Y-Z plane. It is very difficult to make NAV symmetric about X-Z plane while building. This gives rise to non-zero values of J_{xy} and J_{yz}. However, this value will be very small compared with J_{xz} and hence ignored. In the above explanation, J_{xy} is the vehicle product of inertia about the X and Y body axis (kg·m^2), J_{xz} is the vehicle product of inertia about the X and Z body axis (kg·m^2), and J_{yz} is the vehicle product of inertia about the Y and Z body axis (kg·m^2). Mass and mechanical properties of the vehicle are shown in the **Table I**. This NAV is a fixed wing with two control surfaces, elevator for pitch up and rudder for yaw and roll motion. Battery-powered motor-propeller combination is used for propulsion. Two linear servos are used as actuators for the deflection of the elevator and rudder. Single chip solution of 3-axis rate gyro, 3-axis accelerometer along with the magnetometer is proposed to use as an inertial measurement unit. Motor, servos and instruments are placed inside the vertical fin. The high wing configuration is selected in order to provide more roll stability even under the adverse reaction torque produced by motor-propeller configuration.

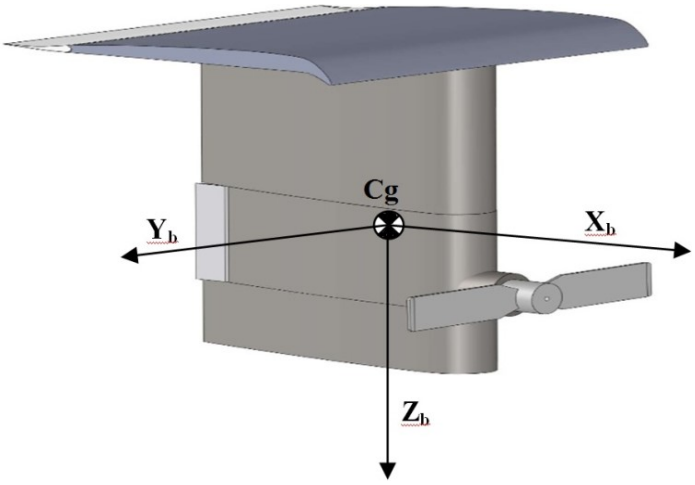

Figure 1 Geometric diagram of NAV

Table I Mass and mechanical properties

Weight (kg)	0.015
Wing Chord (m)	0.075
Wing Span (m)	0.075
Wing Area (m^2)	0.005625
Vertical fin area (m^2)	0.004875
J_{xx} (kg·m^2)	$5.83\cdot10^{-6}$
J_{yy} (kg·m^2)	$9.24\cdot10^{-6}$
J_{zz} (kg·m^2)	$4.93\cdot10^{-6}$
J_{xz} (kg·m^2)	$2.46\cdot10^{-6}$

Aerodynamic characteristics

Rectangular wing planform is used in the NAV. Airfoil for the wing is a modified Eppler 59, and for vertical downside fin, a modified J5012 is used. The aerodynamic coefficient of the NAV is evaluated using XFLR5, which can analyze flow over airfoils, wings and planes operating at low Reynolds number. It generates total lift and drag of the vehicle for different values of α and β, where α is the angle-of-attack (rad) and β is the side-slip angle (rad). XFLR5 also gives various moment components of the vehicle about the center of gravity as a function of α and β values. Using this lift and moment, lateral and longitudinal static coefficients can be derived at a given operating point. All dynamic derivatives are computed by applying theoretical/empirical formulas mentioned in [3],[6], and [9]. The vehicle is simulated in XFLR5 for velocity ranges from 8 to 12 m·s^{-1}. The aerodynamic data obtained from XFLR5 is integrated with Matlab for further analysis. The aerodynamic characteristic of the vehicle for velocity 8 m·s^{-1} is presented below in the form of figures.

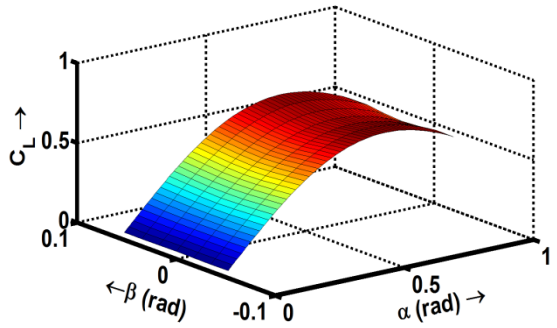

Figure 2 C_L at null elevator deflection

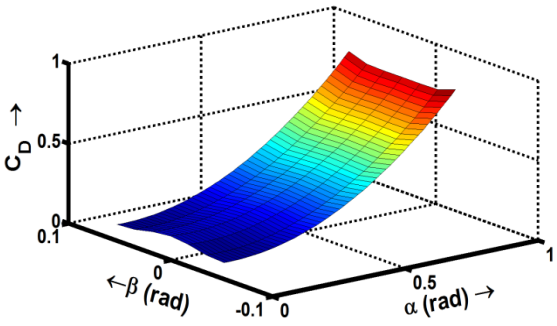

Figure 3 C_D at null elevator deflection

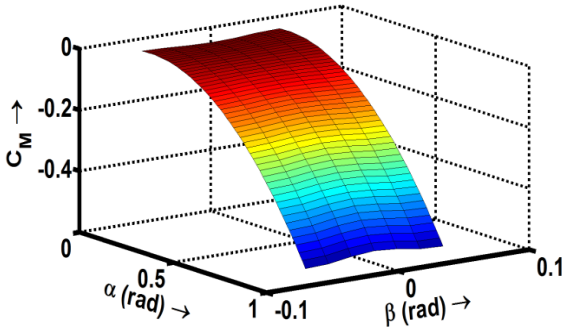

Figure 4 C_M at null elevator deflection

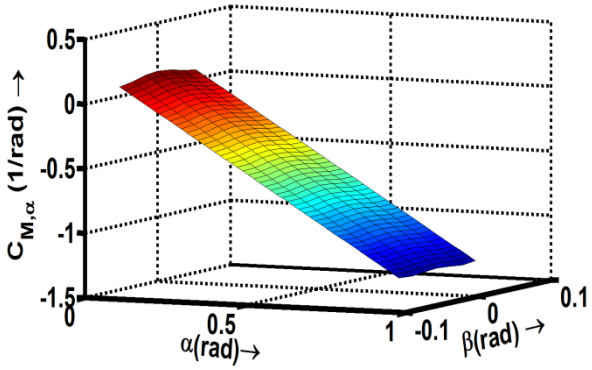

Figure 5 $C_{M,\alpha}$ at null elevator deflection

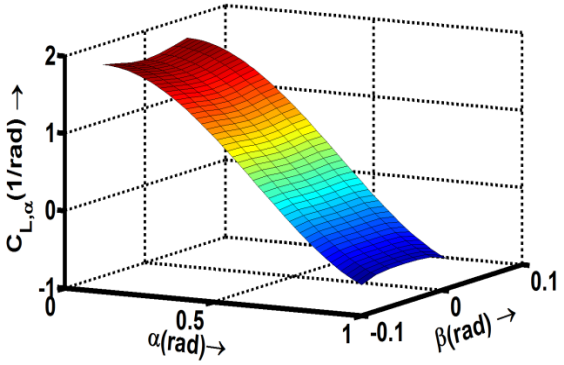

Figure 6 $C_{L,\alpha}$ at null elevator deflection

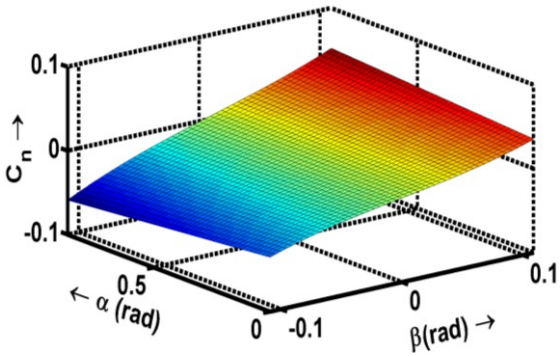

Figure 7 C_n at null rudder deflection

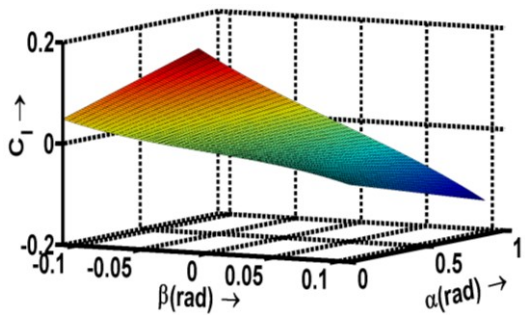

Figure 8 C_l at null rudder deflection

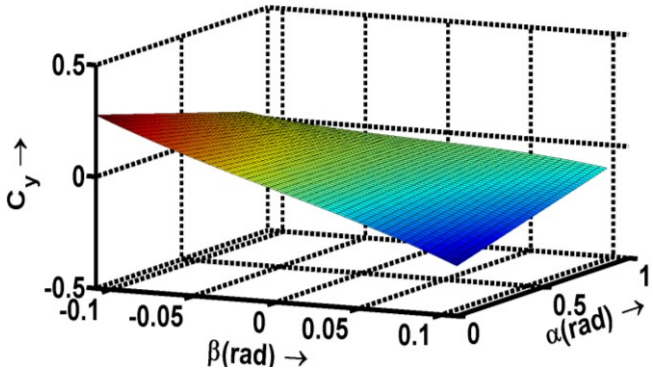

Figure 9 C_y at null rudder deflection

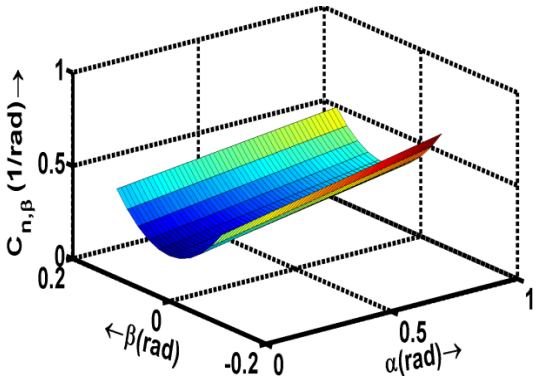

Figure 10 $C_{n,\beta}$ at null rudder deflection

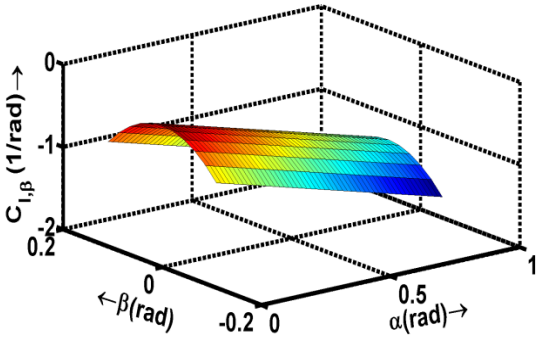

Figure 11 $C_{l,\beta}$ at velocity 8 m·s^{-1}

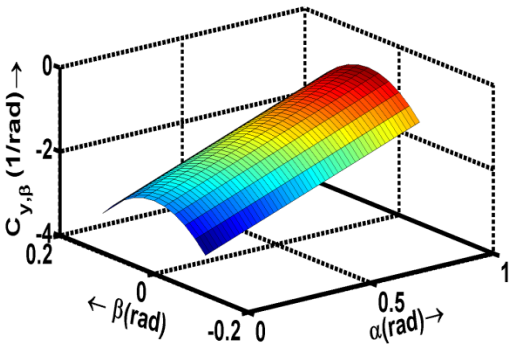

Figure 12 $C_{y,\beta}$ at velocity 8 m·s^{-1}

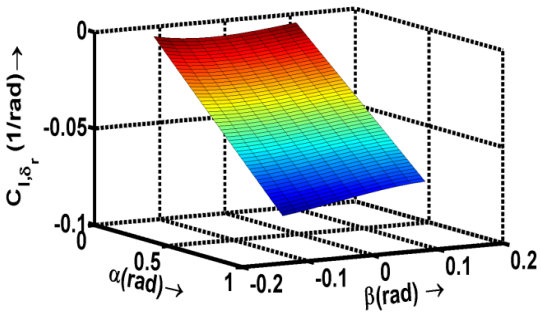

Figure 13 $C_{l\delta r}$ at velocity 8 m·s^{-1}

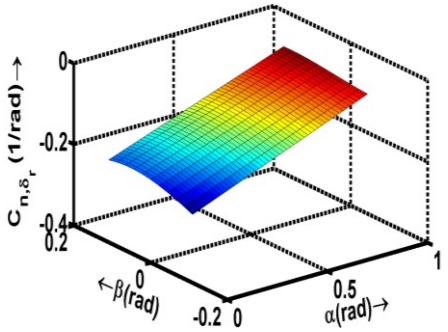

Figure 14 $C_{n,\delta r}$ at velocity 8 m·s^{-1}

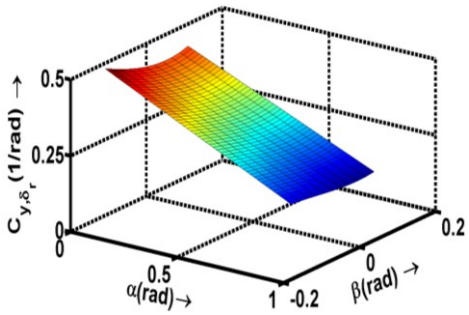

Figure 15 $C_{y,\delta r}$ at velocity 8 m·s^{-1}

The geometric configuration of 75 mm NAV is simulated for ranges of α, β, δ_e and δ_r at different flight speeds, where δ_e, δ_r are elevator deflection (rad), and rudder deflections (rad) respectively. The equations describing the characteristics of static aerodynamic coefficients are obtained by curve fitting aerodynamic data acquired from XFLR5 in terms of α, β, δ_e and δ_r using Matlab. The characteristics of aerodynamic coefficients are shown in various figures in this section.

Figure 2 depicts lift coefficients C_L. The drag coefficient C_D is shown in **Figure 3**. From **Figure 2**, the stall angle-of-attack is at 0.62 (rad) and this is also established from $C_{L,\alpha}$ curve shown in **Figure 6**. The $C_{L,\alpha}$ curve shows that stall angle-of-attack occur when $C_{L,\alpha}$ begin to be negative. Pitching moment coefficient C_M and its derivative are shown in **Figure 4** and **Figure 5**. **Figure 4** shows that C_{m0} is negative and **Figure 5** reveals $C_{m,\alpha}$ is negative for any angle-of-attack above 0.06 (rad). This means that the wing is unbalanced and vehicle can achieve longitudinal static stability for any operating angles-of-attack above 0.06 (rad). Usually due to aerodynamic inefficiency, NAV will be operating at high angles-of-attack so that longitudinal static instability at the small angles-of-attack is not a problem. Yawing moment coefficient C_n, rolling moment coefficient C_l, side-force coefficient C_y, and their derivatives with respect to β are shown in **Figure 7** to **Figure 12**. The requirement of directional and lateral stability is that, $C_{n,\beta}$ should be positive and $C_{l,\beta}$ must be negative, and the **Figure 10** and **Figure 11** show the same. Change in side-force coefficient due to change in side-slip angle $C_{y,\beta}$ is shown in **Figure 12**. Behavior of cross control derivative $C_{l,\delta r}$, primary control derivative (rudder control power) $C_{n,\delta r}$, and the change in side-force coefficient resulting from a rudder deflection $C_{y,\delta r}$ are shown in **Figure 13** to **Figure 15**. Analyzing the behavior of $C_{n,\delta r,}$ and $C_{y,\delta r}$ establishes that positive rudder deflection produces negative yawing moment and positive side-force, which matches with the traditional results. But $C_{l,\delta r}$ is negative, which means that positive rudder deflection produces negative rolling moment. This helps in achieving the coordinated turn. In above explanations, $C_{L,\alpha}$ is the lift coefficient derivative with respect to angle-of-attack (rad^{-1}), C_{m0} is the pitching moment coefficient at zero angle-of-attack, $C_{m,\alpha}$ is the pitching moment coefficient derivative with respect to angle-of-attack (rad^{-1}), $C_{l,\beta}$ is the rolling moment coefficient derivative with respect to side-slip angle (rad^{-1}), and $C_{n,\beta}$ is the yawing moment coefficient derivative with respect to side-slip angle (rad^{-1}).

III. Nonlinear Equations Of Motion

The nonlinear force and moment equations of motion are described from (1) to (16). For the derivation of these equations below, it is assumed that NAV is rigid body and also the moments and products of inertia do not change with time, as no mass is consumed in an electric propulsion system [8]. The gravity gradient torque due to asymmetric weight distribution is very small and hence not considered.

$$\dot{u} = rv - qw - g\sin(\theta) + \frac{X}{m} + \frac{T}{m} \tag{1}$$

$$\dot{v} = pw - ru + g\sin(\phi)\cos(\theta) + \frac{Y}{m} \tag{2}$$

$$\dot{w} = qu - pv + g\cos(\phi)\cos(\theta) + \frac{Z}{m} \tag{3}$$

$$\dot{p} = \frac{J_{zz}}{J_D}[qr(J_{xx} - J_{zz}) + L_A + J_{xz}pq] + \frac{J_{xz}}{J_D}[pq(J_{xx} - J_{yy}) - qrJ_{xz} + N_A] \tag{4}$$

$$\dot{q} = \frac{1}{J_{yy}}[pr(J_{zz} - J_{xx}) + J_{xz}(r^2 - p^2) + M_A + M_T] \tag{5}$$

$$\dot{r} = \frac{J_{xz}}{J_D}[qr(J_{yy} - J_{zz}) + J_{xz}pq + L_A] + \frac{J_{xx}}{J_D}[pq(J_{xx} - J_{yy}) - J_{xz}qr + N_A] \tag{6}$$

where J_{xx} is the vehicle moment of inertia about the X body axis (kg·m^2), J_{yy} is the vehicle moment of inertia about the Y body axis (kg·m^2), J_{zz} is the vehicle moment of inertia about the Z body axis (kg·m^2), L_A denotes aerodynamic rolling moment

(N·m), M_A is aerodynamic pitching moment (N·m), m is the mass of the vehicle (kg), M_T is the pitching moment due to thrust (N·m), N_A is aerodynamic yawing moment (N·m), u indicates the X axis component of velocity in the body-fixed reference frame ($m \cdot s^{-1}$), v is the Y axis component of velocity in the body-fixed reference frame ($m \cdot s^{-1}$), w is the Z axis component of velocity in the body-fixed reference frame ($m \cdot s^{-1}$), p is roll angular velocity in the body-fixed reference frame ($rad \cdot s^{-1}$), q is pitch angular velocity in the body-fixed reference frame ($rad \cdot s^{-1}$), r is yaw angular velocity in the body-fixed reference frame ($rad \cdot s^{-1}$), T denotes thrust (N), ϕ is the bank angle, θ indicates pitch angle (rad), and $J_D = J_{xx}J_{zz} - J_{xz}^2$.

The above force and moment equations consist of aerodynamic, thrust, and gravitational force and moment components. The aerodynamic force components expressed in body axis are as follows:

$$X = -\mathcal{D}\cos(\alpha)\cos(\beta) - \mathcal{Y}\cos(\alpha)\sin(\beta) + \mathcal{L}\sin(\alpha) \quad (7)$$

$$Y = \mathcal{D}\sin(\beta) + \mathcal{Y}\cos(\beta) \quad (8)$$

$$Z = -\mathcal{D}\sin(\alpha)\cos(\beta) - \mathcal{Y}\sin(\alpha)\sin(\beta) - \mathcal{L}\cos(\alpha) \quad (9)$$

where $\mathcal{L}$ is lift force in wind axis (N), $\mathcal{D}$ is drag force in wind axis (N), and $\mathcal{Y}$ denotes the side-force in wind axis (N). The drag, lift, side-force, aerodynamic and thrust moments are defined as follows.

$$\mathcal{D} \equiv QSC_D(\alpha, \beta, \delta_e)$$

$$\mathcal{L} \equiv QSC_L(\alpha, \beta, \delta_e)$$

$$\mathcal{Y} \equiv QSC_y(\alpha, \beta, \delta_r)$$

$$M_A \equiv QScC_m(\alpha, \beta, \delta_e)$$

$$L_A \equiv QScC_l(\alpha, \beta, \delta_r)$$

$$N_A \equiv QScC_n(\alpha, \beta, \delta_r)$$

$$M_T \equiv T(\delta_T)Z_T$$

where Q is the dynamic pressure ($N \cdot m^{-2}$), S is reference area (m^2), c is chord length (m), δ_T is the speed control signal for the motor (s) and Z_T is the Z axis location of the thrust from center of gravity (m).

The aerodynamic coefficients C_L, C_D, C_y, C_l, C_m and C_n are expressed as a nonlinear function with respect to α and β. The angle-of-attack, side-slip angle and magnitude of vehicle's velocity are defined as

$$\alpha = \tan^{-1}\left(\frac{w}{u}\right) \quad (10)$$

$$\beta = \sin^{-1}\left(\frac{v}{V}\right) \quad (11)$$

$$V = \sqrt{u^2 + v^2 + w^2} \quad (12)$$

Along with force and moment equations, three kinematics equations and one navigational equation are used to define equations of motion of the NAV. These equations are expressed below:

$$\dot{\phi} = p + q\sin(\phi)\tan(\theta) + r\cos(\phi)\tan(\theta) \quad (13)$$

$$\dot{\theta} = q\cos(\phi) - r\sin(\phi) \quad (14)$$

$$\dot{\psi} = q\sin(\phi)\sec(\theta) + r\cos(\phi)\sec(\theta) \quad (15)$$

$$\dot{h} = u\sin(\theta) - v\sin(\phi)\cos(\theta) - w\cos(\phi)\cos(\theta) \quad (16)$$

where ψ, $h$are heading angle (rad) and height of the vehicle above sea level (m).

Equations (1) to (6) along with (13) to (16) are used for trim calculations, as well as these equations are utilized to derive coupled and uncoupled lateral-longitudinal linear equations around an equilibrium flight condition.

IV. Linearized Equations Of Motion

Linear equations of motion are found by taking Jacobians of equations of motion, both for lateral and longitudinal dynamics about a trim condition.

Lateral Equations

For the lateral state-space equations, the state variable is given by [8].

$$x_{lat} \triangleq (\bar{v}, \bar{p}, \bar{r}, \bar{\phi})^T$$

and input scalar is defined as

$$u_{lat} \triangleq (\bar{\delta}_r)$$

The Jacobians of (2), (4), (6), and (13) are given by

$$\begin{bmatrix} \dot{\bar{v}} \\ \dot{\bar{p}} \\ \dot{\bar{r}} \\ \dot{\bar{\phi}} \end{bmatrix} = \begin{bmatrix} \frac{\partial \dot{v}}{\partial v} & \frac{\partial \dot{v}}{\partial p} & \frac{\partial \dot{v}}{\partial r} & \frac{\partial \dot{v}}{\partial \phi} \\ \frac{\partial \dot{p}}{\partial v} & \frac{\partial \dot{p}}{\partial p} & \frac{\partial \dot{p}}{\partial r} & \frac{\partial \dot{p}}{\partial \phi} \\ \frac{\partial \dot{r}}{\partial v} & \frac{\partial \dot{r}}{\partial p} & \frac{\partial \dot{r}}{\partial r} & \frac{\partial \dot{r}}{\partial \phi} \\ \frac{\partial \dot{\phi}}{\partial v} & \frac{\partial \dot{\phi}}{\partial p} & \frac{\partial \dot{\phi}}{\partial r} & \frac{\partial \dot{\phi}}{\partial \phi} \end{bmatrix} \begin{bmatrix} \bar{v} \\ \bar{p} \\ \bar{r} \\ \bar{\phi} \end{bmatrix} + \begin{bmatrix} \frac{\partial \dot{v}}{\partial \delta_r} \\ \frac{\partial \dot{p}}{\partial \delta_r} \\ \frac{\partial \dot{r}}{\partial \delta_r} \\ \frac{\partial \dot{\phi}}{\partial \delta_r} \end{bmatrix} \begin{bmatrix} \bar{\delta}_r \end{bmatrix} \quad (17)$$

Using the stability derivative notations, linearized state space equations can be written as

$$\begin{bmatrix} \dot{\bar{v}} \\ \dot{\bar{p}} \\ \dot{\bar{r}} \\ \dot{\bar{\phi}} \end{bmatrix} = \begin{bmatrix} Y_v & Y_p & Y_r & Y_\phi \\ L_v & L_p & L_r & 0 \\ N_v & N_p & N_r & 0 \\ 0 & 1 & \phi_r & \phi_\phi \end{bmatrix} \begin{bmatrix} \bar{v} \\ \bar{p} \\ \bar{r} \\ \bar{\phi} \end{bmatrix} + \begin{bmatrix} Y_{\delta_r} \\ L_{\delta_r} \\ N_{\delta_r} \\ 0 \end{bmatrix} \begin{bmatrix} \bar{\delta}_r \end{bmatrix} \quad (18)$$

where

$$Y_\phi = g\cos(\phi_0)\cos(\theta_0) \quad (19)$$

$$\phi_r = \cos(\phi_0)\tan(\theta_0) \quad (20)$$

$$\phi_\phi = q\cos(\phi_0)\tan(\theta_0) - r\sin(\phi_0)\tan(\theta_0) \quad (21)$$

and in the above equations, ϕ_0, and θ_0 are trim values of bank angle and pitch angle.

Longitudinal Equations

For the longitudinal state-space equations, the state variable and control inputs are given by [9].

$$x_{long} \triangleq (\bar{u}, \bar{w}, \bar{q}, \bar{\theta})^T$$

$$u_{long} \triangleq (\bar{\delta}_e, \bar{\delta}_T)^T$$

The corresponding linearized state-space equations are given by

$$\begin{bmatrix}\dot{\bar{u}}\\ \dot{\bar{w}}\\ \dot{\bar{q}}\\ \dot{\bar{\theta}}\end{bmatrix}=\begin{bmatrix}X_u & X_w & X_q & X_\theta\\ Z_u & Z_w & Z_q & Z_\theta\\ M_u & M_w & M_q & 0\\ 0 & 0 & \theta_r & 0\end{bmatrix}\begin{bmatrix}\bar{u}\\ \bar{w}\\ \bar{q}\\ \bar{\theta}\end{bmatrix}+\begin{bmatrix}X_{\delta_e} & X_{\delta_T}\\ Z_{\delta_e} & 0\\ M_{\delta_r} & M_{\delta_T}\\ 0 & 0\end{bmatrix}\begin{bmatrix}\bar{\delta}_e\\ \bar{\delta}_T\end{bmatrix} \quad (22)$$

where

$$X_\theta = -g\cos(\theta_0) \quad (23)$$

$$Z_\theta = -gsin(\theta_0)\,cos(\phi_0) \quad (24)$$

$$\theta_q = \cos(\phi_0) \quad (25)$$

These conventional linearized equations neglect the coupling between longitudinal and lateral dynamics. However, this assumption is not strictly valid that can be seen in the following description.

Coupled Equations

For coupled lateral-longitudinal state-space equations, the states are given by

$$x \triangleq (\bar{u}, \bar{v}, \bar{w}, \bar{p}, \bar{q}, \bar{r}, \bar{\theta}, \bar{\phi})^{\mathrm{T}}$$

and input vector is defined as

$$u \triangleq (\bar{\delta}_e, \bar{\delta}_T, \bar{\delta}_r)^{\mathrm{T}}$$

The Jacobian of coupled equations are expressed below

$$\begin{bmatrix}\dot{\bar{u}}\\ \dot{\bar{v}}\\ \dot{\bar{w}}\\ \dot{\bar{p}}\\ \dot{\bar{q}}\\ \dot{\bar{r}}\\ \dot{\bar{\theta}}\\ \dot{\bar{\phi}}\end{bmatrix}=\begin{bmatrix}\frac{\partial\dot{u}}{\partial u} & \frac{\partial\dot{u}}{\partial v} & \frac{\partial\dot{u}}{\partial w} & \frac{\partial\dot{u}}{\partial p} & \frac{\partial\dot{u}}{\partial q} & \frac{\partial\dot{u}}{\partial r} & \frac{\partial\dot{u}}{\partial\theta} & \frac{\partial\dot{u}}{\partial\phi}\\ \frac{\partial\dot{v}}{\partial u} & \frac{\partial\dot{v}}{\partial v} & \frac{\partial\dot{v}}{\partial w} & \frac{\partial\dot{v}}{\partial p} & \frac{\partial\dot{v}}{\partial q} & \frac{\partial\dot{v}}{\partial r} & \frac{\partial\dot{v}}{\partial\theta} & \frac{\partial\dot{v}}{\partial\phi}\\ \frac{\partial\dot{w}}{\partial u} & \frac{\partial\dot{w}}{\partial v} & \frac{\partial\dot{w}}{\partial w} & \frac{\partial\dot{w}}{\partial p} & \frac{\partial\dot{w}}{\partial q} & \frac{\partial\dot{w}}{\partial r} & \frac{\partial\dot{w}}{\partial\theta} & \frac{\partial\dot{w}}{\partial\phi}\\ \frac{\partial\dot{p}}{\partial u} & \frac{\partial\dot{p}}{\partial v} & \frac{\partial\dot{p}}{\partial w} & \frac{\partial\dot{p}}{\partial p} & \frac{\partial\dot{p}}{\partial q} & \frac{\partial\dot{p}}{\partial r} & \frac{\partial\dot{p}}{\partial\theta} & \frac{\partial\dot{p}}{\partial\phi}\\ \frac{\partial\dot{q}}{\partial u} & \frac{\partial\dot{q}}{\partial v} & \frac{\partial\dot{q}}{\partial w} & \frac{\partial\dot{q}}{\partial p} & \frac{\partial\dot{q}}{\partial q} & \frac{\partial\dot{q}}{\partial r} & \frac{\partial\dot{q}}{\partial\theta} & \frac{\partial\dot{q}}{\partial\phi}\\ \frac{\partial\dot{r}}{\partial u} & \frac{\partial\dot{r}}{\partial v} & \frac{\partial\dot{r}}{\partial w} & \frac{\partial\dot{r}}{\partial p} & \frac{\partial\dot{r}}{\partial q} & \frac{\partial\dot{r}}{\partial r} & \frac{\partial\dot{r}}{\partial\theta} & \frac{\partial\dot{r}}{\partial\phi}\\ \frac{\partial\dot{\theta}}{\partial u} & \frac{\partial\dot{\theta}}{\partial v} & \frac{\partial\dot{\theta}}{\partial w} & \frac{\partial\dot{\theta}}{\partial p} & \frac{\partial\dot{\theta}}{\partial q} & \frac{\partial\dot{\theta}}{\partial r} & \frac{\partial\dot{\theta}}{\partial\theta} & \frac{\partial\dot{\theta}}{\partial\phi}\\ \frac{\partial\dot{\phi}}{\partial u} & \frac{\partial\dot{\phi}}{\partial v} & \frac{\partial\dot{\phi}}{\partial w} & \frac{\partial\dot{\phi}}{\partial p} & \frac{\partial\dot{\phi}}{\partial q} & \frac{\partial\dot{\phi}}{\partial r} & \frac{\partial\dot{\phi}}{\partial\theta} & \frac{\partial\dot{\phi}}{\partial\phi}\end{bmatrix}\begin{bmatrix}\bar{u}\\ \bar{v}\\ \bar{w}\\ \bar{p}\\ \bar{q}\\ \bar{r}\\ \bar{\theta}\\ \bar{\phi}\end{bmatrix}+\begin{bmatrix}\frac{\partial\dot{u}}{\partial\delta_e} & \frac{\partial\dot{u}}{\partial\delta_T} & \frac{\partial\dot{u}}{\partial\delta_r}\\ \frac{\partial\dot{v}}{\partial\delta_e} & \frac{\partial\dot{v}}{\partial\delta_T} & \frac{\partial\dot{v}}{\partial\delta_r}\\ \frac{\partial\dot{w}}{\partial\delta_e} & \frac{\partial\dot{w}}{\partial\delta_T} & \frac{\partial\dot{w}}{\partial\delta_r}\\ \frac{\partial\dot{p}}{\partial\delta_e} & \frac{\partial\dot{p}}{\partial\delta_T} & \frac{\partial\dot{p}}{\partial\delta_r}\\ \frac{\partial\dot{q}}{\partial\delta_e} & \frac{\partial\dot{q}}{\partial\delta_T} & \frac{\partial\dot{q}}{\partial\delta_r}\\ \frac{\partial\dot{r}}{\partial\delta_e} & \frac{\partial\dot{r}}{\partial\delta_T} & \frac{\partial\dot{r}}{\partial\delta_r}\\ \frac{\partial\dot{\theta}}{\partial\delta_e} & \frac{\partial\dot{\theta}}{\partial\delta_T} & \frac{\partial\dot{\theta}}{\partial\delta_r}\\ \frac{\partial\dot{\phi}}{\partial\delta_e} & \frac{\partial\dot{\phi}}{\partial\delta_T} & \frac{\partial\dot{\phi}}{\partial\delta_r}\end{bmatrix}\begin{bmatrix}\bar{\delta}_e\\ \bar{\delta}_T\\ \bar{\delta}_r\end{bmatrix} \quad (26)$$

The linearized state-space coupled equations are given below

$$\begin{bmatrix}\dot{\bar{u}}\\ \dot{\bar{v}}\\ \dot{\bar{w}}\\ \dot{\bar{p}}\\ \dot{\bar{q}}\\ \dot{\bar{r}}\\ \dot{\bar{\theta}}\\ \dot{\bar{\phi}}\end{bmatrix}=\begin{bmatrix}X_u & X_v & X_w & X_p & X_q & X_r & X_\theta & 0\\ Y_u & Y_v & Y_w & Y_p & 0 & Y_r & Y_\theta & Y_\phi\\ Z_u & Z_v & Z_w & Z_p & Z_q & Z_r & Z_\theta & Z_\phi\\ L_u & L_v & L_w & L_p & L_q & L_r & 0 & 0\\ M_u & M_v & M_w & M_p & M_q & M_r & 0 & 0\\ N_u & N_v & N_w & N_p & N_q & N_r & 0 & 0\\ 0 & 0 & 0 & 0 & \theta_q & \theta_r & 0 & \theta_\phi\\ 0 & 0 & 0 & 1 & \phi_q & \phi_r & \phi_\theta & 0\end{bmatrix}\begin{bmatrix}\bar{u}\\ \bar{v}\\ \bar{w}\\ \bar{p}\\ \bar{q}\\ \bar{r}\\ \bar{\theta}\\ \bar{\phi}\end{bmatrix}+\begin{bmatrix}X_{\delta_e} & X_T & X_{\delta_r}\\ Y_{\delta_e} & 0 & Y_{\delta_r}\\ Z_{\delta_e} & 0 & Z_{\delta_r}\\ L_{\delta_e} & 0 & L_{\delta_r}\\ M_{\delta_e} & M_T & 0\\ N_{\delta_e} & 0 & N_{\delta_r}\\ 0 & 0 & 0\\ 0 & 0 & 0\end{bmatrix}\begin{bmatrix}\bar{\delta}_e\\ \bar{\delta}_T\\ \bar{\delta}_r\end{bmatrix} \quad (27)$$

where

$$X_\theta = -g\cos(\theta_0) \quad (28)$$

$$Y_\theta = -gsin(\phi_0)\,cos(\theta_0) \quad (29)$$

$$Y_\phi = gcos(\phi_0)\,cos(\theta_0) \quad (30)$$

$$Z_\theta = -gsin(\theta_0)\,cos(\phi) \quad (31)$$

$$Z_\phi = -gsin(\phi_0)\,cos(\theta_0) \quad (32)$$

$$\theta_q = \cos(\phi_0) \quad (33)$$

$$\theta_r = -sin(\phi_0) \quad (34)$$

$$\theta_\phi = -qsin(\phi_0) - r\cos(\phi_0) \quad (35)$$

$$\phi_q = sin(\phi_0)\,tan(\theta_0) \quad (36)$$

$$\phi_r = cos(\phi_0)\,tan(\theta_0) \quad (37)$$

$$\phi_\theta = qsin(\phi_0)\sec^2(\theta_0) + r\,cos(\phi)\sec^2(\theta_0) \quad (38)$$

$$\phi_\phi = -qcos(\phi_0)\,tan(\theta_0) - rsin(\phi)\,tan(\theta_0) \quad (39)$$

V. Simulation Results And Discussions

This section discusses trim analysis and stability analysis of NAV.

Trim analysis

The analysis of the flight dynamics of NAVs begins with trim analysis. The trim solution is the steady-state solution of the nonlinear (1) to (6) and (13) to (16). Flight condition considered here is a steady turn with a steady climb. This flight condition involves both climbing and turning, with turn radius of 30 m and rate of climb equals to 1 m·s^{-1}. Trim solution is calculated for different flight velocities ranging from 8 to 12 m·s^{-1}. **Figure 16** and **Figure 17** show thrust required and trim angle-of-attack for various specified trim conditions.

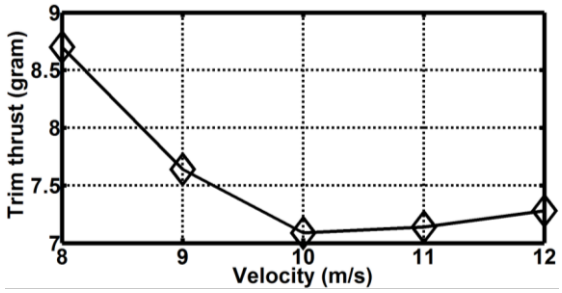

Figure 16 Thrust required curve

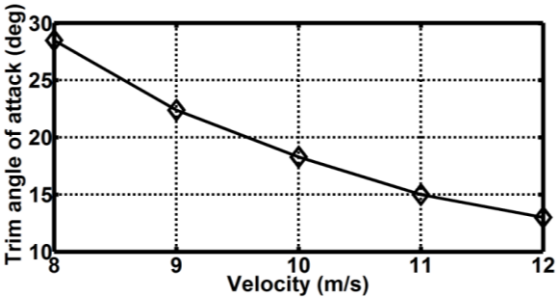

Figure 17 Trim angle of attack

At velocities of 12 m·s^{-1}, required thrust is less than those at 8 and 9 m·s^{-1} because at high velocities, the drag is mainly due to dynamic pressure. As velocity decreases from 12 m·s^{-1}, drag due to dynamic pressure reduces and hence required thrust decreases initially. In order to support the weight as velocity decreases, lift is raised by increasing angle-of-attack, thereby increasing induced drag, which is proportional to the square of lift coefficient. This elevates total drag and consequently, required thrust increases rapidly.

Other important performance measures of NAV that can be evaluated using the steady-state solution are endurance and range. Expression for the estimation of endurance and range of battery-powered aircraft is given below [10].

$$E = \left[\frac{\eta_{tot} V_B C}{0.5 \rho S V^3 C_D}\right]^n \tag{40}$$

$$R_E = E \times V \tag{41}$$

where E is the estimated endurance (hour), η_{tot} is the combined efficiency of motor and propeller, V_B is the voltage of the battery (volts), C denotes battery capacity (A·h), ρ indicates density of the air (kg·m^{-3}), n is the discharge parameter of battery and R_E is the estimated range (m).

Endurance and range for different flight velocity as a function of η_{tot} is shown in **Figure 18** (**a** and **b**) with 130 mA·h LiPo battery. For the NAV, required endurance is 5 minutes and range is 500 m. The plot shows battery capacity is more than what is actually needed to meet endurance and range requirements. This is because (40) and (41) calculate endurance and range, which depend only on drag and thereby calculated thrust required. In reality, the battery has to supply power to autopilot, sensors, actuators and communication devices, which reduces the range and endurance considerably from the values calculated by endurance and range equations. Considering this, 130 mA·h LiPo battery is chosen.

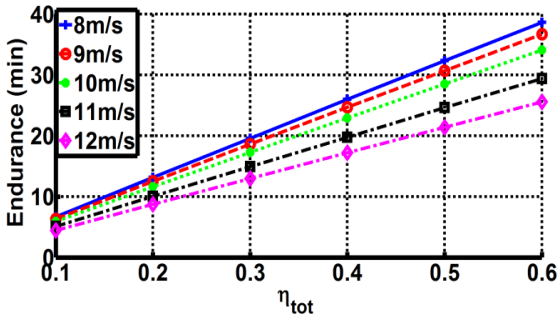

(a) Estimated Endurance of nano air vehicle

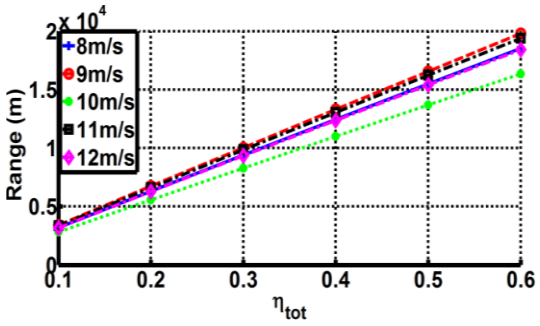

(b) Estimated Range of nano air vehicle

Figure 18 Performance characteristic of nano air vehicle

Stability analysis

This part explains the stability analysis of both coupled and uncoupled linear lateral-longitudinal system for the trim flight speed 8 m·s^{-1}. For stability analysis of NAV, the linear coupled and uncoupled state-space models given in (18), (22), and (27) are considered. The system and input matrix of uncoupled lateral and longitudinal dynamics at the flight speed 8 m·s^{-1} are given below.

$$A_{lat} = \begin{bmatrix} Y_v & Y_p & Y_r & Y_\phi \\ L_v & L_p & L_r & 0 \\ N_v & N_p & N_r & 0 \\ 0 & 1 & \phi_r & \phi_\phi \end{bmatrix} = \begin{bmatrix} -2.38 & 3.82 & -7.02 & 7.76 \\ -226.80 & -2.09 & 1.93 & 0 \\ 17.78 & -0.27 & -0.67 & 0 \\ 0 & 1 & 0.67 & 0 \end{bmatrix} \tag{42}$$

$$B_{lat} = \begin{bmatrix} Y_{\delta_r} \\ L_{\delta_r} \\ N_{\delta_r} \\ 0 \end{bmatrix} = \begin{bmatrix} 3.63 \\ -323.80 \\ -496.50 \\ 0 \end{bmatrix} \tag{43}$$

$$A_{long} = \begin{bmatrix} X_u & X_w & X_q & X_\theta \\ Z_u & Z_w & Z_q & Z_\theta \\ M_u & M_w & M_q & 0 \\ 0 & 0 & \theta_r & 0 \end{bmatrix} = \begin{bmatrix} -0.19 & 0.08 & -3.79 & -8.04 \\ -0.89 & -2.53 & 7.07 & -5.42 \\ 28.51 & -132.20 & -1.16 & 0 \\ 0 & 0 & 0.97 & 0 \end{bmatrix} \tag{44}$$

$$B_{long} = \begin{bmatrix} X_{\delta_e} & X_{\delta_T} \\ Z_{\delta_e} & 0 \\ M_{\delta_r} & M_{\delta_T} \\ 0 & 0 \end{bmatrix} = \begin{bmatrix} -0.41 & 0.47 \\ -8.67 & 0 \\ -1015 & 11.45 \\ 0 & 0 \end{bmatrix} \quad (45)$$

Similarly, system and input matrix of the coupled model is expressed below.

$$A = \begin{bmatrix} X_u & X_v & X_w & X_p & X_q & X_r & X_\theta & 0 \\ Y_u & Y_v & Y_w & Y_p & 0 & Y_r & Y_\theta & Y_\phi \\ Z_u & Z_v & Z_w & Z_p & Z_q & Z_r & Z_\theta & Z_\phi \\ L_u & L_v & L_w & L_p & L_q & L_r & 0 & 0 \\ M_u & M_v & M_w & M_p & M_q & M_r & 0 & 0 \\ N_u & N_v & N_w & N_p & N_q & N_r & 0 & 0 \\ 0 & 0 & 0 & 0 & \theta_q & \theta_r & 0 & \theta_\phi \\ 0 & 0 & 0 & 1 & \phi_q & \phi_r & \phi_\theta & 0 \end{bmatrix}$$

$$= \begin{bmatrix} -0.19 & 0.27 & 0.08 & 0 & -3.79 & 0.005 & -8.04 & 0 \\ -0.22 & -2.38 & -0.15 & 3.82 & 0 & -7.02 & -1.46 & 7.76 \\ -0.89 & 0.19 & -2.53 & -0.005 & 7.08 & 0 & -5.415 & -2.09 \\ 0.28 & -226.8 & -0.43 & -2.09 & 0.12 & 1.93 & 0 & 0 \\ 28.51 & 1.11 & -132.20 & 0.06 & -1.16 & 0.13 & 0 & 0 \\ 0.43 & 17.78 & -0.79 & -0.27 & 0.058 & -0.67 & 0 & 0 \\ 0 & 0 & 0 & 0 & 0.97 & -0.26 & 0 & -0.22 \\ 0 & 0 & 0 & 1 & 0.18 & 0.67 & 0.33 & 0 \end{bmatrix} \quad (46)$$

$$B = \begin{bmatrix} X_{\delta_e} & X_T & X_{\delta_r} \\ Y_{\delta_e} & 0 & Y_{\delta_r} \\ Z_{\delta_e} & 0 & Z_{\delta_r} \\ L_{\delta_e} & 0 & L_{\delta_r} \\ M_{\delta_e} & M_T & 0 \\ N_{\delta_e} & 0 & N_{\delta_r} \\ 0 & 0 & 0 \\ 0 & 0 & 0 \end{bmatrix} = \begin{bmatrix} -0.41 & 0.47 & -0.002 \\ -0.003 & 0 & 3.63 \\ -8.67 & 0 & -0.001 \\ -0.01 & 0 & -323.8 \\ -1015 & 11.45 & 0 \\ -0.08 & 0 & -496.5 \\ 0 & 0 & 0 \\ 0 & 0 & 0 \end{bmatrix} \quad (47)$$

The dynamic analysis of the NAV is done by studying the eigenvalues and eigenvectors of the system matrix of the coupled and uncoupled linear model. **TABLE II** shows the eigenvalues of coupled and decoupled lateral-longitudinal system.

From the result given in **Table II**, it is evident that lateral-longitudinal coupling has a strong influence to the damping of the phugoid mode. The roll, short period, and Dutch roll modes are almost totally unaffected by the coupling. The most significant change can be observed in the spiral mode. In the uncoupled system spiral mode is stable, whereas it is unstable in the coupled system. The effect of coupling on the phugoid mode and spiral mode is even more dramatically demonstrated by examining the eigenvectors. **Table III** shows the phugoid mode and spiral mode eigenvectors belongs to coupled and uncoupled lateral-longitudinal system.

By analyzing the eigenvectors of spiral mode in uncoupled case, the results look traditional where it is governed by ϕ, r and p. A substantially different result is observed in coupled case where spiral mode has a dominant contribution from u, ϕ, r, q, p, w, θ and v. Similarly, phugoid mode in the coupled system receives dominant contributions from p and ϕ along with u, which is the major contributor. This is a contrasting behavior compared with the conventional uncoupled system where phugoid mode is mainly influenced by u.

Table II Comparison between eigenvalues: with and without coupling in steady turn and climb flight

Mode	Without coupling	With coupling
	Eigenvalues	Eigenvalues
Phugoid	-0.197 ± 1.12j	-0.312 ± 1.26j
Short period	-1.74 ± 32.3j	-1.75 ± 32.3j
Dutch roll	-1.15 ± 31.5j	-1.17 ± 31.5j
Roll	-2.68	-2.73
Spiral	-0.149	0.194

Table III Phugoid and roll mode steady turn and climb eigenvectors with and without coupling

Eigen vector component	Phugoid mode		Spiral mode	
	with coupling	without coupling	with coupling	without coupling
$\bar{u}$	-0.9020	-0.9590	0.7129	0
$\bar{v}$	0.0010 ± 0.0029j	0	0.0060	0.0085
$\bar{w}$	-0.1929 ± 0.0006j	-0.2055 ± 0.0008j	0.1521	0
$\bar{p}$	-0.2422 ± 0.0459j	0	-0.1822	-0.4632
$\bar{q}$	-0.1123 ± 0.0895j	-0.1399 ± 0.0515j	0.1909	0
$\bar{r}$	0.0169 ± 0.1320j	0	0.4114	0.5305
$\bar{\theta}$	0.0379 ± 0.0995j	0.06364 ± 0.1094j	-0.1225	0
$\bar{\phi}$	0.1125 ± 0.1615j	0	0.4633	0.7099

Damping ratio and natural frequency of phugoid mode in the coupled and uncoupled model are portrayed on the **Figure 19** (**a** and **b**). The phugoid mode damping ratio for uncoupled lateral-longitudinal system is increasing with velocity. This phenomenon is illustrated in **Figure 19** (**a**). On the other hand, for a coupled model, phugoid mode damping ratio is somewhat settling to a value. This feature is very important and need in-depth investigation, as it is extremely difficult to understand the behavior of the coupled model by analyzing the uncoupled model. The natural frequency of phugoid mode is higher for coupled system compared with the uncoupled system as shown in **Figure 19** (**b**).

Variation of spiral mode poles with trim velocity is illustrated in **Figure 20**. It shows that at high velocity, the coupled and uncoupled poles are almost same. As the velocity decreases, the difference between coupled and uncoupled spiral poles increases. This is because of the coupling effect which becomes influential at low velocity due to increase in trim angle-of-attack. In order to understand the behavior of phugoid mode and spiral mode characteristics shown in **Figure 19** and **Figure 20**, further investigation of the system is needed. By investigating the eigenvalues, it is found that spiral mode is unstable, and Dutch roll damping is very poor. To improve spiral mode and Dutch mode characteristics and their performance measures simultaneously, yaw damping has to increase, which has a favorable impact on both. Yaw damping can be improved by bringing geometric changes to vehicle or by a feedback control system which provides additional yaw damping.

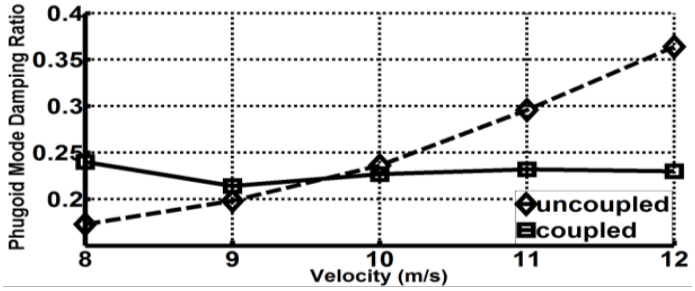

(a) Phugoid damping ratio, $\zeta_{n_{ph}}$

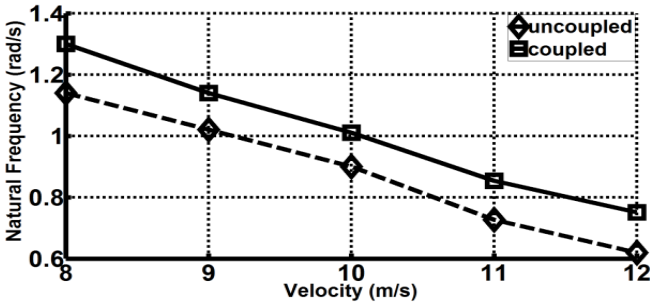

(b) Phugoid natural frequency, $\omega_{n_{ph}}$

Figure 19 Dynamic characteristic of phugoid mode

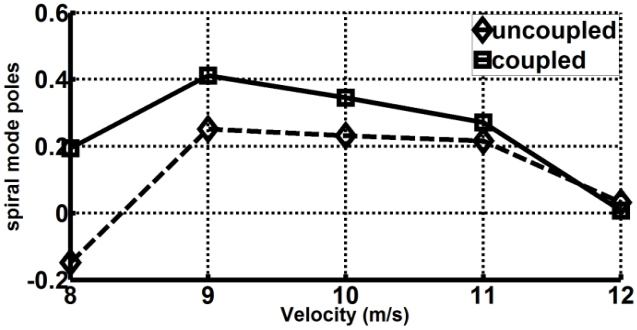

Figure 20 Spiral mode characteristics

The geometric changes which improve yaw damping also increase yaw stability, which has an adverse effect upon the spiral mode. The better solution is to employ an electronic damper, which can be constructed by using a rate gyro that produces an output signal proportional to yaw rate of the vehicle. So by employing full state feedback, assuming all states are available for feedback, performance of spiral and Dutch roll mode can be improved simultaneously. Desired poles are given by

$$P = [-10 \pm 32.3j \;\; -10 \pm 31.5j \;\; -2.73 \;\; -1 \pm 1.26j \;\; -0.194] \quad (48)$$

By pole placement, desired feedback gain matrix is given below.

$$K = \begin{bmatrix} 00.18 & -0.37 & 0.045 & 0.026 & -0.79 & 0.02 & -0.04 & 0.17 \\ 20.92 & -28.31 & -7.60 & 2.13 & -69.53 & 0.92 & 5.90 & 15.57 \\ -0.003 & 0.07 & 0.0005 & 0.03 & -0.004 & -0.05 & -0.01 & 0.055 \end{bmatrix} \quad (49)$$

Feedback effectiveness is tested by giving a disturbance to the coupled and decoupled system with a pulse disturbance of pulse width 0.25 s and magnitude -0.0175. **Figure (a to h)** depict the response of both coupled and decoupled systems to this pulse disturbance.

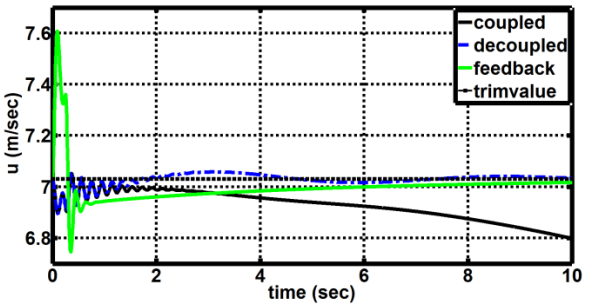

(a) Velocity component u

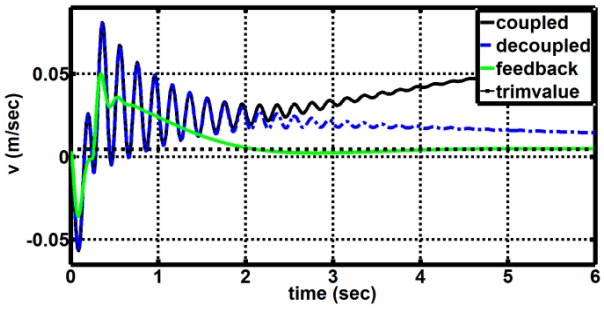

(b) Velocity component v

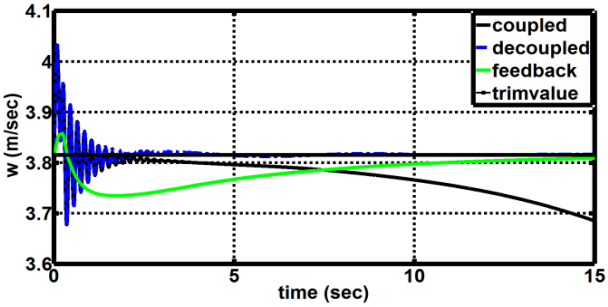

(c) Velocity component w

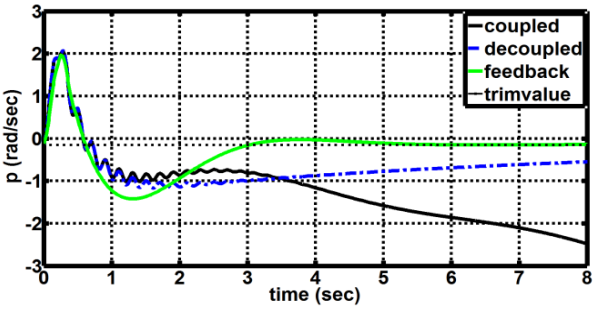

(d) Roll rate p

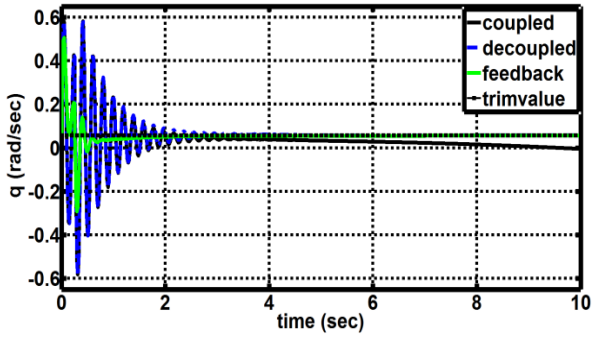

(e) Pitch rate q

Figure 21 Response of Coupled and Uncoupled system for pulse disturbance

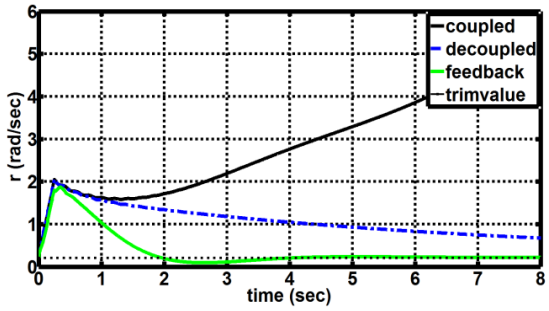

(f) yaw rate r

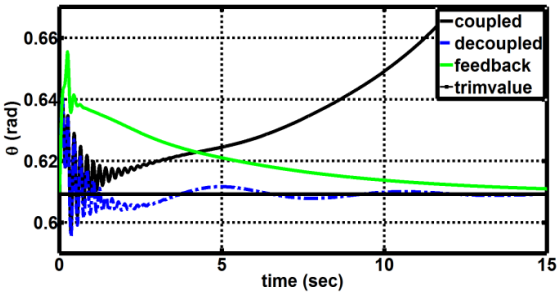

(g) Pitch angle θ

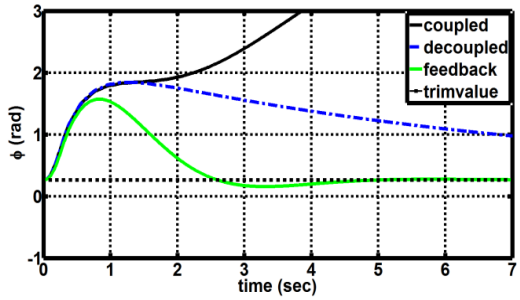

(h) Bank angle ϕ

Figure 21 Response of Coupled and Uncoupled system for pulse disturbance (continued)

VI. CONCLUSIONS

In the present study, flight dynamics modeling and analysis of a NAV has been presented. From the results presented here, the lateral-longitudinal coupling under steady turn and climb flight has a significant effect upon the NAV dynamics. It has been concluded from this study that the lateral-longitudinal coupling associated with turning flight of the NAV can significantly alter the phugoid and the spiral mode, even with the exclusion of the propeller effect from the aerodynamic coupling. During the study, it is found that spiral mode remains unstable and Dutch roll damping remain poor for this configuration of the NAV for coupled model. To improve spiral and Dutch mode characteristic simultaneously, feedback is employed. Further study is needed to understand rotating propeller effect upon the vehicle flight dynamics which will have profound influence in lateral-longitudinal coupling. Furthermore, new study is required to create a better approximate model for different modes so that influence of various parameters and coefficients on the distinct modes of the vehicle can be clearly understood under coupled conditions, which have significant influence in nano and micro flight.

ACKNOWLEDGMENT

This study is funded by NP-MICAV program of DRDO. Good amount of support came from Arun Joseph, Eobin Alex George, Hari Kumar K, Sidhant Dhall and Titas Behra.

REFERENCES

[1] T.J. Mueller, J.C. Kellogg, P.G. Ifju and S.V. Shkarayev, "Introduction to The Design of Fixed-Wing Micro Air Vehicles", AIAA Education Series, AIAA, New York, 2006.

[2] K. Zeal-Sain, S. Chyi-Yeou and C. Yun-Sheng, "Dynamic Modeling and Analysis of A Whole-Wing Microvehicle", in proceedings of AIAA/ASME/ASCE/AHS/ASC Structures, Structural Dynamics, and Material Conference, Honolulu, Hawaii, 2007, AIAA 2007-2238. CrossRef

[3] R.C. Nelson, "Small Disturbance Theory", Flight Stability and Automatic Control 2nd ed., McGraw-Hill, New York, 1998, pp. 104-108.

[4] B.N. Pamadi, "Equations of Motion with Small Disturbance", Performance, Stability, Dynamics, and Control of Airplanes, AIAA, Reston, VA, 1988, pp. 372-375.

[5] T. Yechout, R. (ed.), "Introduction to Aircraft Flight Mechanics: Performance, Static Stability, Dynamic Stability, and Classical Feedback Control", AIAA Education Series, AIAA, Reston, Virginia, 2006.

[6] W.F. Phillips, and B.W. Santana, "Aircraft Small Disturbance Theory with Longitudinal-Lateral Coupling", Journal of Aircraft, Vol. 39, No. 6, Nov-Dec, 2002, pp. 973-980. CrossRef

[7] R.F. Stengel, "Flight Dynamics", 1st Indian edition, Overseas Press, New Delhi, 2009.

[8] R.W. Beard, and T.W. McLain, "Linear Design Models, Navigation, Guidance and Control of Small Unmanned Aircraft", Princeton University Press, New Jersey, 2009, pp. 81-88.

[9] J. Roskam, "Airplane Design: Part 1-VII", Design, Analysis and Research Corporation, Kansas, U.S.A., 1986.

[10] L.W. Traub, "Range and Endurance Estimates for Battery-Powered Aircraft", Journal of Aircraft, Vol. 48, No. 2, March-April, 2011, pp. 703-707. CrossRef